



POLITECNICO
MILANO 1863

**SCUOLA DI INGEGNERIA INDUSTRIALE
E DELL'INFORMAZIONE**

EXECUTIVE SUMMARY OF THE THESIS

Prompt gamma imaging with a slit camera for range monitoring in carbon ion radiation therapy: A Monte Carlo feasibility study.

LAUREA MAGISTRALE IN NUCLEAR ENGINEERING - INGEGNERIA NUCLEARE

Author: ANDREA MISSAGLIA

Advisor: PROF. CARLO ETTORE FIORINI

Co-advisors: AICHA BOURKADI IDRISI, FRANCESCO CASAMICIELA

Academic year: 2021-2022

1. Introduction

Particle therapy has become a promising option for tumor treatments, alternative to surgery, chemotherapy, conventional radiotherapy, and immunotherapy. The main advantage of charged particles over photons is their characteristic dose distribution, which culminates at a maximum called Bragg peak, followed by a steep fall-off. Since most of the dose is located around a peak with limited full-width-at-half-maximum, charged particles allow to precisely hit the tumor site sparing deeper normal tissues. However, their intrinsic precision given by the characteristic dose distribution can be a double-edged sword, as particle range is not exempted from uncertainties which are closely related to the imperfect knowledge of the patient morphology [3]. For this reason, if the beam is not well localized, the consequence may be a non-effective treatment of the pathology, putting in danger nearby normal tissues, therefore making the advantageous feature of hadrontherapy not fully exploitable.

Due to range uncertainties, safety margins are taken in the treatment planning, and this limits the full benefits of particle therapy. Recently, to improve the precision and restrain the irradi-

ation of normal tissues, instruments have been developed with the aim to monitor the particle range *in-vivo* with an ideal precision of few millimeters [4]. The first clinical application was achieved by a proton range verification system [5], which exploited the method of range verification called Prompt Gamma Imaging (PGI), related to the Prompt Gamma-rays (PGs) emitted by the de-excitation of target nuclei after inelastic nuclear reactions.

Over the past few years, there has been a substantial progress in the application of PGI mostly for what concern proton therapy. On the contrary, less improvements have been made in the use of PGI verification within Carbon Ion Radiation Therapy (CIRT). Indeed, even if there are undoubted advantages of C-ions over proton and photon therapy, some C-ions interaction properties may hinder the application of PGI monitoring: for instance, the higher neutron production yield and the smaller number of incident projectiles needed to provide a prescribed dose than for protons strongly affect the signal-to-noise ratio. Hence, the optimization of detection efficiency and gamma-neutron discrimination is even more critical for the application of PGI in CIRT.

In the present thesis, two numerical studies were carried out using the FLUKA general purpose Monte Carlo code for particle transport (version 4-1.1) [1]. The first was a preliminary work with the aim to explore the secondary emission of a tissue-equivalent target irradiated with different beams, while the second study investigated the feasibility of applying PGI in CIRT, using a knife-edge camera. Finally, a possible instrumental set-up was proposed to validate the numerical results in future experiments. Specific attention was given to the readout electronics.

2. Monte Carlo simulations

2.1. Preliminary study

The first numerical study compared the secondary emission and the energy deposition of 200MeV protons, $200\frac{\text{MeV}}{u}$ He-ions and $385\frac{\text{MeV}}{u}$ C-ions; these energies were selected inside the interval of clinical treatments, imposing the same theoretical particle range.

The simulation geometry was composed by a target of tissue equivalent material (soft tissue, ICRP), inside an air-filled room surrounded by walls made of Portland cement. The target was cut in 16 slices to investigate the secondary emission at different depths along the beam direction, i.e., the z axis. These slices had different dimensions, 3cm in the proximal part of the depth-dose distribution and 1cm around the Bragg peak.

As expected, C-ions gave the highest linear energy transfer, followed by He-ions and protons. All the beams produced similar photon lines, which resulted more intense for higher atomic number. One could recognize the 511keV due to positron annihilation and the 2.2MeV due to neutron capture on hydrogen (the most intense for a tissue-equivalent material), but there were also present the most important PG lines for PGI, namely:

- The 4.44MeV line due to ^{16}O and ^{12}C ;
- The 5.2MeV peak given by the superposition of 4 different lines due to reactions with ^{16}O ;
- The 6.129MeV line due to ^{16}O .

This preliminary study also showed quantitatively the higher yield of PG and neutron production for C-ions than for protons, and the quasi-isotropic emission of gamma radiation in

contrast to the forward peaked neutron emission. Finally, it also demonstrated that PG emission is considered by MC code FLUKA and the most important PG lines are included in its library.

2.2. Feasibility study

To investigate the viability of using the PGI technique in carbon ion irradiation, three sets of numerical simulations were performed. Specifically, I scored the response of a pixelated knife-edge slit camera to the secondary particles emitted by a ICRP soft tissue phantom emulating the patient (Figure 1(Left)) irradiated with a beam of C-ions. The generic simulation geometry is showed in Figure 1(Right). A mono-energetic pencil beam of C-ions of $150\frac{\text{MeV}}{u}$, which fits the interval of therapeutic energies used in CIRT [2], was directed along the z -axis of the frame of reference towards one of the faces of the phantom, a square cylinder of 30cm diameter made of ICRP soft tissue. The irradiated face of the phantom was positioned at 5cm on the z -axis, which was labelled as "no-shift" position, where the dose peak is almost centered on the origin of the reference frame.

The detection system of reference for the simulations was partly derived from a gamma camera already developed and characterized in previous studies for proton therapy [4]. The present simulated camera consisted of a knife-edge collimator and a pixelated detector. The former was made of a tungsten alloy and was 4cm thick on the radial direction and 30cm wide along the beam axis. The knife-edge slit was 6mm wide and had a 63° aperture angle. Then, the detector was an array of 16 pixels made of $\text{Lu}_{1.8}\text{Y}_{0.2}\text{SiO}_5$ (LYSO) scintillation material, distributed along the beam axis with a pixel pitch of 6mm. Each pixel was a 10 cm wide strip with a 3cm thickness. As shown in Figure 1(Right), the slit and the face of the detector were placed at a distance of 25cm and 50cm from the z -axis, respectively, giving a field-of-view of 10cm on the phantom. The detector and the slit were centered on the origin of the frame of reference to maximize the PG signal. The whole set-up was defined inside a spherical room of 4m radius filled with air. Let us now dig into the specific features of the three

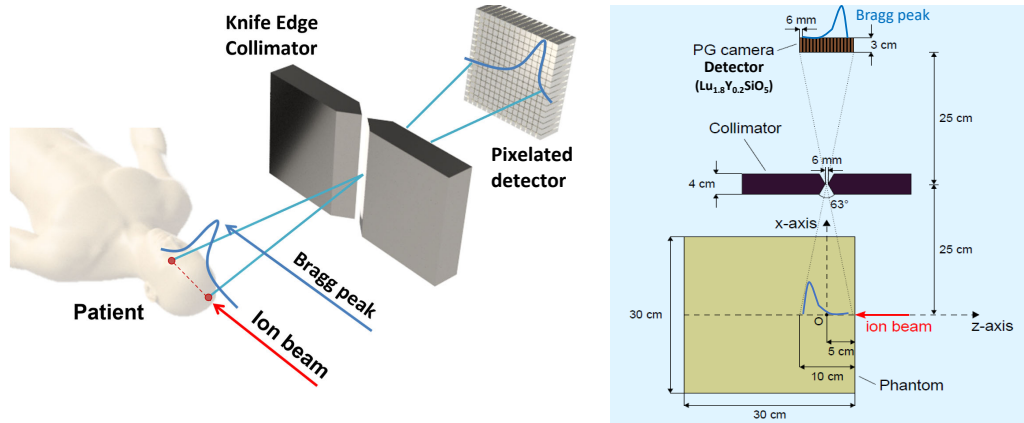


Figure 1: Left. Knife-edge slit prompt-gamma camera with a beam of C-ions hitting a patient. The dose distribution (Bragg peak) is reported on the patient, which is then inverted inside the detector; **Right.** Detailed 2D representation of simulation geometry.

simulation sets:

- 1. First set of simulations.** For this set of simulations, a 3D representation of the set-up is reproduced in Figure 1(Left). From the “no-shift” position the phantom was translated with a 2mm step both in the positive and negative direction of the z-axis, effectively shifting the position of the Bragg peak. The aim of these simulations was two-fold. First, I investigated whether the spatial correlation between the Bragg peak position and the signal profile along the beam axis was visible even in the high neutron background of CIRT. Secondly, I explored the theoretical limits of the specific set-up in determining the C-ion range with the delivery of a single irradiation spot to the phantom, for different numbers of incident carbon ions (10^6 , 10^7 , 10^8 and 10^{10}).
- 2. Second set of simulations.** In the second set of simulations, I evaluated the response of the gamma camera to the delivery of multiple irradiation spots (nine spots as in Figure 2) within a single layer of the phantom, shifting the ion beam axis along the xy-plane but keeping its energy constant. This emulates what happens in pencil beam scanning systems of synchrotron-based treatment facilities, in which the several spots composing a given energy layer are delivered via single cycle, or spill, of the accelerator.
- 3. Third set of simulations.** The non-planar shape of the patient surface and the

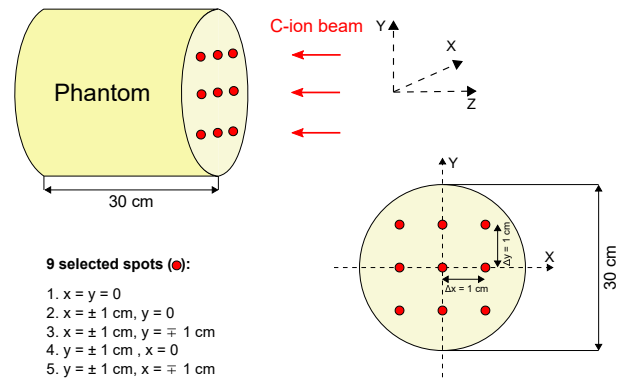


Figure 2: Distribution of the pencil beam spots in space, for carbon ion beam irradiating the soft tissue ICRP phantom.

inhomogeneities introduce a variation in the beam range from spot-to-spot. To account for this, the homogeneous cylindrical phantom was inclined with respect to the z-axis by an angle of 22° . The detector geometry and the selected spots were still those described in the previous set.

The analysis to determine the theoretical accuracy in the range retrieval of the PG camera was based on an algorithm composed by three autonomous parts. In the first part, I obtained the curve representing the total number of counts (or events) per unit C-ion in each pixel as a function of the pixel position on the z-axis (blue histogram in Figure 3a). I then chose a given number of incident C-ions, N_i , and I re-normalized by this number the counts in the signal curve, which was labelled as the “reference curve”. In

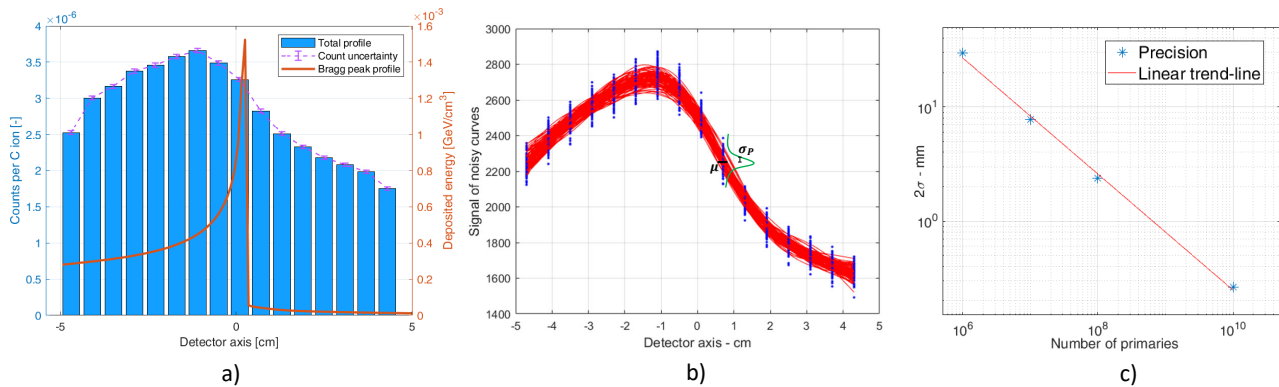


Figure 3: a) Beyond the dose fall-off (orange line), the detection signal (blue histogram) decreases showing the correlation between the detection and the Bragg peak profile; b) Generation of noisy curves exploiting a Poisson sampling; c) Estimated precision as a function of C-ions, defined as 2σ of normal distributions coming from data analysis.

the second part, I performed a propagation of the error on the reference curve. Namely, for each pixel I sampled a given number, N_c , of values from a Poisson distribution having a mean value equal to the number of counts of the reference curve. In this way, I obtained a given set of N_c noisy curves (Figure 3b). Every noisy curve was interpolated with smoothing spline method, to get a continuous curve. 10^4 noisy curves were found to be enough to have a good statistics in the final normal distribution for all methods. The final step of data analysis was to determine the precision of the simulated detection system in retrieving the position of the dose fall-off. Three different methods were employed to compare the obtained noisy curves with the reference one. All the methods brought to a normal frequency distribution, twice standard deviation of which was defined as the precision in retrieving the BP fall-off. The estimated precision was found inversely proportional to the number of C-ions, with a slope of $\approx -\frac{1}{2}$ (Figure 3c).

The first set of simulations brought to two important results: first, the total signal profile was clearly correlated with Bragg peak position, even in the huge neutron background of carbon ion irradiation; secondly, a single pencil beam spot of C-ions was not sufficient to reach the desirable precision of few millimeters on the particle range retrieval, instead typical ion currents of a spill should be considered. For the last two sets of simulations, the analysis was carried out selecting a typical number of carbon ion corresponding to a spill irradiation, namely 5×10^7

ions. From the analysis of the second set of simulations, the estimated theoretical accuracy on particle range, given by the average of the three methods, was 4.2 ± 0.6 mm. For the third set, the resulting precision was 4.4 ± 0.5 mm. In both cases the results seemed in line with the desired precision in the range of few millimeters (4mm target in proton therapy [4]). Hence, it was then demonstrated that, at least on a simulation level in case of a spill irradiation, it is feasible to consider PGs as a useful tool to retrieve the BP fall-off, reducing range uncertainties. Starting from these results, it was natural to think at an experimental campaign to prove the feasibility of PGI technique in CIRT. The proposal of an experimental set-up was the last step of the thesis work.

3. Experimental set-up

3.1. Architecture of the detection system

The purpose of the thesis was to research about the possibility to apply the PGI-technique in carbon ion irradiation. The subsequent step was to experimentally validate what obtained in simulations. In the following, the proposal of a set-up for future experiments is presented.

Due to its superior properties, the scintillation crystal material will be cerium-doped lutetium orthosilicate $\text{Lu}_{1.8}\text{Y}_{0.2}\text{SiO}_5:\text{Ce}$ (LYSO:Ce). Each LYSO crystal will have the dimension of $(1 \times 1)\text{in}^2$, composed by a matrix of 16 pixels with 6.25mm pitch. Two of such crystals will be put one next the other for a to-

tal of 32 pixels and will be read by two 4×4 tiles of SiPM. The selected SiPM tiles will incorporate a SPAD cell size of $(15 \times 15) \mu m^2$, a choice that was dictated by two parameters characterizing the final performances, linearity and speed. With such a high density of cells, the response of the system will be fast enough, and saturation will not constitute a problem.

The gamma-ray energy is firstly split by means of the scintillation crystals into visible photons, which are then converted into electronic charges inside the SiPM tiles constituting the useful analog signal. By a one-on-one coupling between the 16 pixels of a SiPM tile and the 16 analog channels of an ASIC, signals are then managed by an FPGA (field-programmable gate array) after being digitized through ADCs (analog-to-digital converters) mounted on a front-end PCB. To cover the entire area of the gamma camera, one FPGA is necessary. Finally, the collected data will be sent to a host PC through the USB 3.0 connection. In Figure 4, a complete representation of the electronics readout is shown.

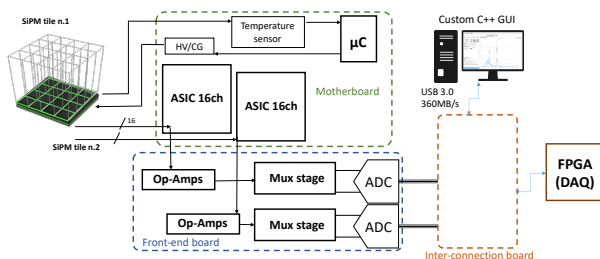


Figure 4: Architecture of the readout electronics, including the motherboard with two ASICs and a micro-controller for gain stabilization, a front-end PCB with a dedicated MUX stage and ADCs; the inter-connection board puts in contact the front-end board with the FPGA-based DAQ and a PC reached by a USB 3.0 connection.

The two SiPM tiles will provide the signal to be processed to the motherboard, which will dispose of temperature sensors and a dedicated high voltage power supply controlled by a micro-controller for gain stabilization; most importantly, the motherboard will contain two custom 16-channel ASICs both for analog and trigger signals. Each analog channel will be associated and managed by a SiPM pixel: they will read the current supplied by the photodetector and will output both a trigger signal for the arrival

time information and an analog voltage signal representing the energy of the gamma-ray in a specific channel.

The motherboard will be directly linked to the FE board by means of suitable connectors, while the inter-connection, DAQ and USB boards will be remotely connected using selected cables. Once the signals are digitized by the ADCs (Figure 4), they will reach the inter-connection board which is needed to connect independent boards, i.e., the evaluation board of the FPGA, front-end board and the one hosting the USB 3.0 connection. Otherwise, it would not be feasible to connect all these boards together.

The front-end PCB has the purpose of digitizing the analog signals coming from the ASICs and to send them to the FPGA. The latter is used as a control system for the front-end PCB: it gathers timing information directly from the trigger signals coming from the ASICs, and manages all the data stream to be sent to the inter-connection board before coming to a custom C++ GUI, by means of a USB 3.0 connection, with a maximum speed of $360 \frac{MB}{s}$. Finally, on the host PC, the information about the gamma detection is associated to the pixel in which the photon was detected, so that the distribution of secondary emissions due to the primary C-ion beam irradiation will be imaged.

3.2. Design of the front-end PCB

The front-end circuit will be developed to read the 32 analog channels coming from the two ASICs, and to convert them into digital data to be provided for the FPGA. Along this path, the 32 analog signals are buffered, multiplexed, and converted into digital values. The trigger lines, instead, provide the information about the arrival time of gamma-rays impinging on the camera and are directly routed from the ASICs to the FPGA.

This board is designed starting from the assumption that the gamma camera will adopt a pixelated LYSO crystal, whose light yield is of $3.32 \times 10^4 \frac{ph}{MeV}$ and the emitted light has a decay time of 36ns with a shape similar to an exponential decay. According to the physical properties of LYSO crystals, it is reasonable to size the detection system in such a way to sustain, for each channel, 5×10^6 counts per second as maximum input rate. This number will drive the choices

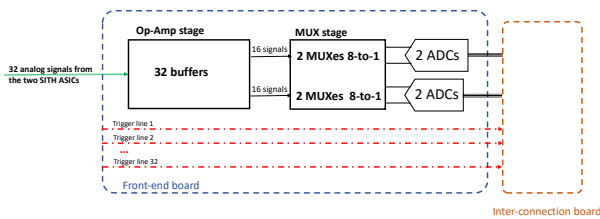


Figure 5: Schematic representation of the blocks composing the FE PCB: an Op-Amp stage, a MUX stage, a block with ADCs. Trigger lines reach the FPGA board with no manipulations.

about the components of the FE board.

In Figure 5, the block diagram of the present PCB is reported. The analog signals, first, are buffered into an Op-Amp stage; then, they move to a MUX stage before being converted into digital signals by the ADCs.

4. Conclusions

In recent years, there has been a substantial progress in the application of PGI mostly for what concern proton therapy. On the other hand, fewer studies have been made in the use of PGI verification for carbon ion radiation therapy. To solve this clear gap in knowledge, the expected goal of this work was to explore the PG fall-off retrieval capability with a well-established slit camera configuration, already tested clinically with proton irradiation.

MC simulations showed that, for the beam energy and the detection system of interest, the signal profile due to the secondary particles emitted from the delivery of a single spot to the phantom was correlated with the BP. Moreover, I demonstrated that the shape of the profile was clearly determined by the prompt-gamma signal over an almost uniform neutron background. The theoretical limitations of our gamma camera were probed investigating the sensitivity in particle range retrieval. From 2mm shifts of the cylindrical target along its axis, the signal curves were clearly distinguishable, opening the possibility to detect 2mm shifts of the BP with a sufficiently high number of incident ions. However, the number of ions delivered in a single spot has proven to be too small for reaching that level of precision, so that this technique is not expected to be effective on a spot-by-spot basis, at least in the considered knife-edge camera configuration.

Thus, I proceeded to verify whether the distal position of the beam in an energy layer could be retrieved with a good accuracy. For this, 5×10^7 ions were used, i.e., the average number of primary particles of an irradiation spill [2]. It was found that a 4mm accuracy is theoretically achievable with the present camera. Even introducing a ± 4 mm beam range variation within the same layer by tilting the phantom, the accuracy was not worsened.

Although our results suggested that range verification on a spot-by-spot basis seems not to be feasible, it may be worth to further investigate the PGI technique in CIRT, at least on single spill basis. Even though a layer-by-layer approach in range verification is not strictly a real-time technique, it could still be useful to reduce the uncertainties during the treatment and for post-treatment verification.

Finally, the conclusions drawn in the present work will be tested in a future experimental campaign, which is currently under organization.

References

- [1] G. Battistoni, T. Boehlen, F. Cerutti, P. W. Chin, L. S. Esposito, A. Fassò, A. Ferrari, A. Lechner, A. Empl, A. Mairani, et al. Overview of the fluka code. *Annals of Nuclear Energy*, 82:10–18, 2015.
- [2] E. Bressi. Operation and patient treatments at cnao facility. *Energy*, 5(C6):O8.
- [3] H. Paganetti. Range uncertainties in proton therapy and the role of monte carlo simulations. *Physics in Medicine & Biology*, 57(11):R99, 2012.
- [4] I. Perali, A. Celani, L. Bombelli, C. Fiorini, F. Camera, E. Clementel, S. Henrotin, G. Janssens, D. Prieels, F. Roellinghoff, et al. Prompt gamma imaging of proton pencil beams at clinical dose rate. *Physics in Medicine & Biology*, 59(19):5849, 2014.
- [5] C. Richter, G. Pausch, S. Barczyk, M. Priegnitz, I. Keitz, J. Thiele, J. Smeets, F. Vander Stappen, L. Bombelli, C. Fiorini, et al. First clinical application of a prompt gamma based in vivo proton range verification system. *Radiotherapy and Oncology*, 118(2):232–237, 2016.